LIMNOLOGY
and
OCEANOGRAPHY: METHODS

Limnol. Oceanogr.: Methods 8, 2010, 424–440

Modeling photosynthesis-irradiance curves: Effects of temperature, dissolved silica depletion, and changing community assemblage on community photosynthesis

Tom J. S. Cox[1,2], Karline Soetaert[2], Jean-Pierre Vanderborght[3], Jacco C. Kromkamp[2], and Patrick Meire[1]*

[1]University of Antwerp, Department of Biology, Ecosystem Management Research Group, Universiteitsplein 1, B-2610 Antwerpen, Belgium

[2]Netherlands Institute of Ecology (NIOO-KNAW), Centre for Estuarine and Marine Ecology, Korringaweg 7, P.O. Box 140, 4400 AC Yerseke, The Netherlands

[3]Université Libre de Bruxelles, Laboratory of Chemical Oceanography and Water Geochemistry, CP 208, Bd du Triomphe, B-1050, Bruxelles, Belgium

Abstract

Sets of photosynthesis-irradiance (P-I) curves yield more information about community photosynthesis when analyzed with proper models in mind. Based on ecosystem-specific considerations regarding the factors that explain spatial and temporal patterns of photosynthesis, the Webb model of photosynthesis can be extended and fitted to P-I data. We propose a method based on a series of nested models of increasing complexity to test whether supposed effects of environmental factors are reflected in the P-I data, whether more complex models fit the data significantly better than more simple models, and whether parameters describing the presumed dependencies can be estimated from the data set. We compare a direct approach, fitting the extended model to all P-I data at once, with a two-step approach in which photosynthetic efficiencies and maximum photosynthetic rates of individual P-I curves are determined first, and then related to environmental variables. A nested model approach prevents overfitting of multiparameter models. Monte Carlo analysis sheds light on the error structure of the model, by separating parameter and model uncertainty, and provides an assessment of the performance of the formulations used in ecosystem models. We demonstrate that the two-step approach underperforms when used to compute photosynthetic rates. We apply the proposed method to an extensive P-I data set from the Schelde estuary, where spatiotemporal patterns of photosynthesis arise from a combination of seasonality, silica depletion, phytoplankton community composition, and salinity effects.

*Corresponding author: E-mail: tom.cox@ua.ac.be

Acknowledgments

Most of this work is financed by the Flemish Government, Environment and Infrastructure department, AWZ, now NV WandZ (NV Waterwegen en Zeekanaal). The OMES monitoring and data management have been possible only by the continuous coordination effort of Stefan Van Damme and Tom Maris (University of Antwerp). We thank Marie Lionard (University of Ghent) for kindly providing the data on community composition. We thank Didier Bajura (Université Libre de Bruxelles [ULB]) for support in sampling. Dissolved silica concentrations were determined by Lieve Clement and Eva De Bruyn in the University of Antwerp, Department of Biology, Testing Laboratory for Chemical Water Quality. Michèle Loijens and Nathalie Roevros (ULB) are gratefully acknowledged for performing ^{14}C experiments and associated analytical determinations. The data analysis and manuscript preparation was done using free software. We are grateful to the free software community for providing such nice software as LaTeX, R, JabRef, and the Gimp. This is publication 4835 of the NIOO-KNAW Netherlands Institute of Ecology.

DOI 10.4319/lom.2010.8.424

Phytoplankton primary production plays a crucial role in a range of local and global phenomena. In the quest for understanding the dynamics of algal growth and its associated processes (nutrient uptake, temperature dependence, photoacclimation, etc.), considerable effort is put into both data gathering and modeling. Two main approaches can be distinguished: on the one hand, carefully designed laboratory experiments allow the growth of selected species to be studied under full control, and more or less complex dynamical models are built and calibrated on the data set (e.g., Geider et al. 1997; Davidson and Gurney 1999; Flynn and Martin-Jezequel 2000). This approach increases our mechanistic understanding (Baklouti et al. 2006), although it is acknowledged that existing data sets are not adequate for the evaluation of detailed models (Flynn and Martin-Jezequel 2000). On the other hand, ecosystem scale studies of whole plankton communities are performed by incubating samples retrieved from the field at ambient conditions and varying light intensities E,

and fitting a photosynthesis-irradiance (P-I) equation for every individual water sample. Next the spatiotemporal properties of the parameters of the P-I curve, of plankton production, and of the trophic status of the ecosystem are studied (e.g. Alpine and Cloern 1988; Keller 1988; Cole 1989; Kromkamp and Peene 1995; MacIntyre and Cullen 1996; Goosen et al. 1999; Gazeau et al. 2005; Goebel and Kremer 2007). Whereas the former approach elucidates the mechanisms underlying algal growth, the performance of the models under (changing) ambient conditions is difficult to assess, since it is virtually impossible to replicate all occurring natural situations in the laboratory. Moreover, these single-species studies cannot simply be translated to an ecosystem scale, where a succession of several species is observed, each with different dynamics and sensitivities to environmental cues. In contrast, the latter approach fully acknowledges the importance of natural variability in algal community and environmental complexity, but fails in incorporating more detailed (mechanistic) knowledge in analyzing P-I data under varying temperature, nutrient availability, and community composition.

Usually, the relation of algal photosynthesis to environmental factors is studied in two steps. First, individual P-I curves are fitted, which retrieves photosynthesis parameters such as photosynthetic efficiency and maximal photosynthesis rate. Second, these derived parameters are regressed against environmental factors. In this article, we present two alternative approaches for analyzing P-I measurements. In one approach, the *direct* procedure, parameters from an extended Webb model (Webb et al. 1974) are estimated by fitting to all P-I and relevant environmental data at once. This extended Webb model describes community photosynthesis as depending on light and other environmental variables. In the second approach, the *two-step* procedure, the classic photosynthesis parameters α and P_m from each P-I curve are estimated first. Subsequently, these estimates are considered "observed data" and used to fit models that are derived from the models in the first approach. For both approaches, a series of nested models of increasing complexity is used to test whether the supposed effects of environmental factors are reflected in the data, whether the more complex model fits the data significantly better, and whether the parameters describing the presumed dependencies can be estimated from the data set.

Such analyses would provide useful tools to study spatiotemporal patterns of community photosynthesis linked to environmental factors. In estuaries, for example, with a gradient from saline to freshwater tidal reaches, such spatial variability is pronounced. Concomitant with the abiotic gradient, the biological features such as algal community composition and its properties change along the estuary (Kromkamp and Peene 1995; Muylaert et al. 2000; Goebel and Kremer 2007). Similarly, in both abiotic and biotic parameters, a strong seasonality is often observed, reflecting direct responses to ambient temperatures but also resulting from seasonal succession of plankton species. Finally, periods of nutrient limitation would influence community photosynthesis and potentially be reflected in observed P-I curves.

We apply the proposed methods to an extensive P-I data set from freshwater and brackish reaches of the Schelde estuary, gathered during 2003–2004. The monthly P-I determinations along the estuarine axis provide an elaborate data set of 151 P-I curve determinations totaling 1204 photosynthesis irradiance measurements. The system is known for its spatial gradient, recurring silica depletion, and seasonal changes in phytoplankton community composition, and therefore this data set is ideally suited to assess and illustrate the subtleties of the proposed methods. Accordingly, we demonstrate that effects on community photosynthesis of seasonality, silica depletion, and community composition lead to changes in the P-I curve that are predictable to a certain extent. We compare the results of the direct and the two-step approaches, where we focus on their different performances for the calculation of photosynthetic rates. The formulations we use are commonly used in ecosystem model studies, although they are mainly inspired by results of single-species experiments. Therefore we pay considerable attention to the interpretation of the results and their potential use. A Monte Carlo analysis of parameter and model uncertainty provides an assessment of the performance of the formulations used in model calculations of ecosystem photosynthesis.

Materials and procedures

Study area—The Schelde estuary is situated in Northern Belgium and the Southwest of the Netherlands (Fig. 1). The total area draining into the estuary is about 22,000 km^2. The tidal wave enters deeply inland, resulting in about 240 km of estuarine reaches experiencing a macro tidal regime. The estuary exhibits the unique transition from salt over brackish to freshwater tidal areas (Meire et al. 2005). Weirs blocking the tidal wave determine the upstream boundaries of the estuary. Since 1995, the main freshwater (FW) branch has been intensively monitored as part of the Onderzoek naar de Milieueffecten van het SIGMA plan (OMES; Research on the environmental effects of the SIGMA plan) project: monthly samples are taken at ~6-km intervals (Table 1 and Fig. 1) (Van Damme et al. 2005; Cox et al. 2009).

Photosynthesis—Photosynthesis was studied at nine sampling stations along the estuary with ^{14}C incubation (Steemann Nielsen 1951). During 2003–2004, in total 151 water samples were analyzed on a monthly basis, the winter months December, January, and February excluded. Of these samples, 97 originated from the freshwater tidal reach (salinity <1). As such, 1204 photosynthesis-irradiance data points were obtained, 776 of them from the freshwater tidal reach. Samples were transported to the lab in the dark and on ice and were incubated within 4 h after sampling.

In each water sample, a solution of $H^{14}CO_3^-$ (1 mL of 45 µCi mL^{-1} in 600 mL sample) was spiked. After mixing, five 1-mL subsamples were withdrawn from the spiked solution, immedi-

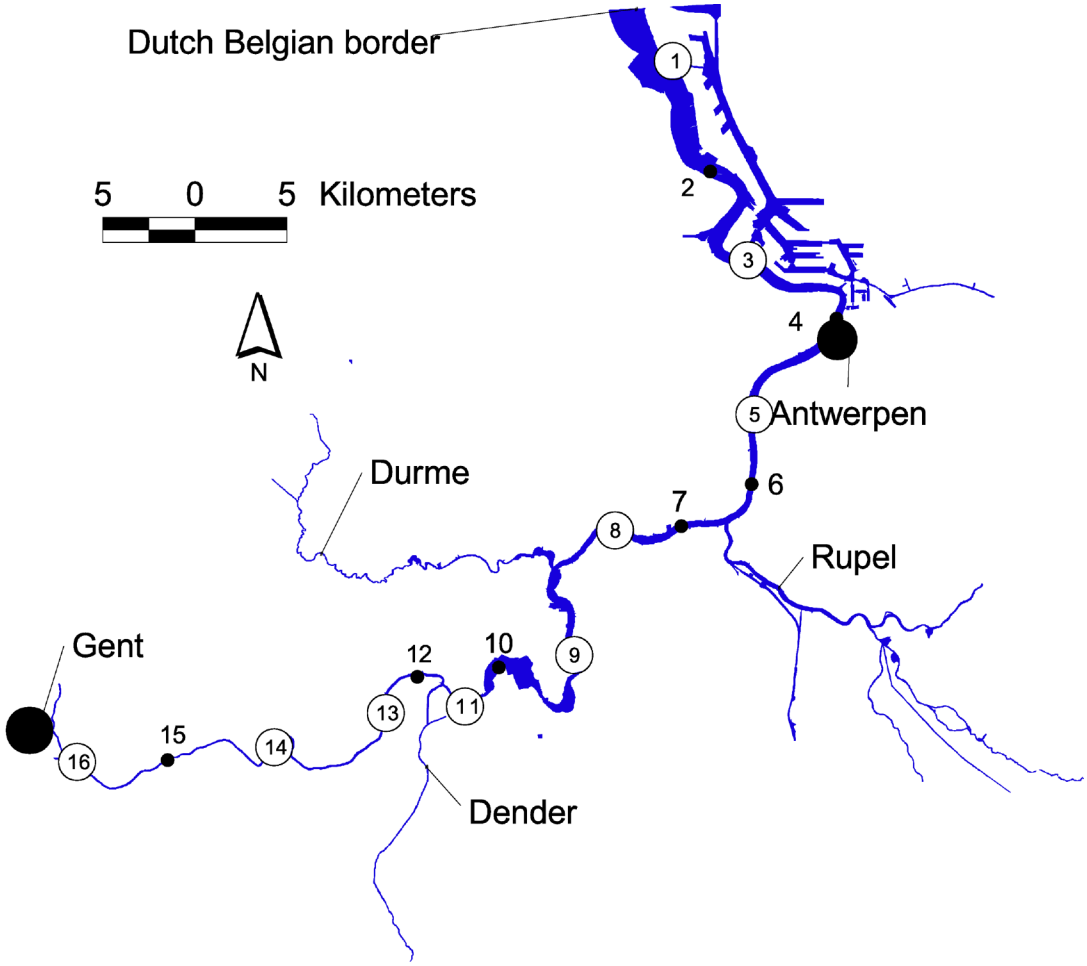

Fig. 1. The Belgian part of the Schelde estuary with its tributaries and major cities. Numbers indicate the sampling stations of the OMES monitoring campaign. Encircled numbers indicate stations where photosynthetic rates were determined.

ately treated with 500 µL NaOH 0.1 N, and analyzed for total ^{14}C activity (see below). The average from the five measurements was used as the initial ^{14}C activity at the beginning of the incubation. At the same time, nine 50-mL subsamples were taken and transferred into Corning incubation flasks for the measurements of ^{14}C uptake by phytoplankton. One of the subsamples was used for the determination of dark ^{14}C uptake by autotrophs, and the other eight were placed in a four-rank incubator fixed on a shaking plate. Each rank held a series of eight aligned flasks, the first being directly exposed to the light source (Sylvania Daylight F 8W/D); with this arrangement, the light intensity decreased from the first to the eighth flask in each rank. The irradiance was measured in the flasks using a quantum scalar irradiance meter (Biospherical Instruments QSL 2100). Typical light profiles ranged from 400–500 to 20–50 µmol photons m^{-2} s^{-1}, depending on the water turbidity. Maximal light intensity reflected the maximal in situ light availability. At the end of the incubation period (between 2 and 3 h), the flask contents were filtered on GF/F glass-fiber filters (pore size 0.7 µm). Filters were acidified with 100 µL HCl 0.1 N to eliminate the remaining bicarbonate before being dried and transferred to scintillation vials. The ^{14}C activity was determined in a liquid scintillation analyzer (Packard 1600 TR) after addition of a scintillation cocktail (Ready Safe, Beckman Coulter).

Other laboratory methods—Chlorinity was determined colorimetrically, from which salinity was calculated as $S = 0.03 + 1.805 * Cl$ [g L^{-1}] (Unesco 1985). DSi samples were stored at 4°C and analyzed by inductively coupled plasma optical emission spectrometry (ICP-OES) within 24 h after sampling. Average winter (Dec–Feb) DSi concentration in the FW tidal reaches amounted to 247 µM in 2003 and 253 µM in 2004, whereas the observed minima in summer were 1.3 and 0.8 µM, respectively. DSi concentrations <10 µM, taken as a conservative upper limit for possible silica limitation (Martin-Jezequel et al. 2000), were observed in both years in an extended part of the FW tidal reaches (Fig. 2A). In situ measured temperature displayed a clear seasonality (Fig. 2B): mean winter (summer) temperature in 2003 was 5.8°C (22.7°C) and 6.4°C

Table 1. The OMES monitoring stations.

Name	Number	Distance, km	Salinity
Boei 87[a]	1	58	9.5
Boei 92	2	63.5	6.6
Boei 105	3	71	4.1
Antwerpen	4	78	2.0
Kruibeke[a]	5	85	0.80
Bazel	6	89	0.53
Steendorp	7	94	0.40
Temse[a]	8	98.5	0.30
Mariekerke[a]	9	107	0.20
Vlassenbroek	10	118	0.18
Dendermonde[a]	11	121	0.17
St-Onolfs	12	125	0.17
Appels[a]	13	128	0.17
Uitbergen[a]	14	138	0.17
Wetteren	15	145	0.17
Melle[a]	16	151	0.17

The distance is from the mouth of the estuary (Vlissingen, Netherlands). Salinity is the 2003–2004 average.
[a]Stations where photosynthesis parameters were determined.

(20.9°C) in 2004.

Except for June–October 2003, chlorophyll *a* (chl *a*) concentrations (Fig. 3C) were determined with HPLC analysis. Sampled water (250–500 mL) was filtered over a GF/F glass fiber filter (Whatmann). Filters were wrapped in aluminum foil and stored on ice during transport and at –80°C in the lab. Pigments were extracted in 90% acetone by means of sonication (tip sonicator, 40 W for 30 s). Pigment extracts were filtered over a 0.2-µm nylon filter and injected into a Gilson HPLC system equipped with an Alltima reverse-phase C18 column (25 cm × 4.6 mm, 5 µm particle sizes). Pigments were analyzed according to Wright and Jeffrey (1997). This method uses a gradient of three solvents: methanol 80%–ammonium acetate 20%, acetonitrile 90%, and ethyl acetate. We used an Applied Biosystems 785A detector to measure absorbance at 685 nm, a Gilson model 121 fluorometer to measure fluorescence of chlorophylls and their derivates, and a Gilson 170 diode array detector to measure absorbance spectra for individual pigment peaks. Pigments were identified by comparison of retention times and absorption spectra with pure pigment standards.

June–October 2003 chl *a* concentrations were determined fluorometrically. Phytoplankton cells were collected by filtration on GF/F glass fiber filters (nominal pore size 0.7 µm) and were then deep-frozen and kept in the dark at –15°C. Chloro-

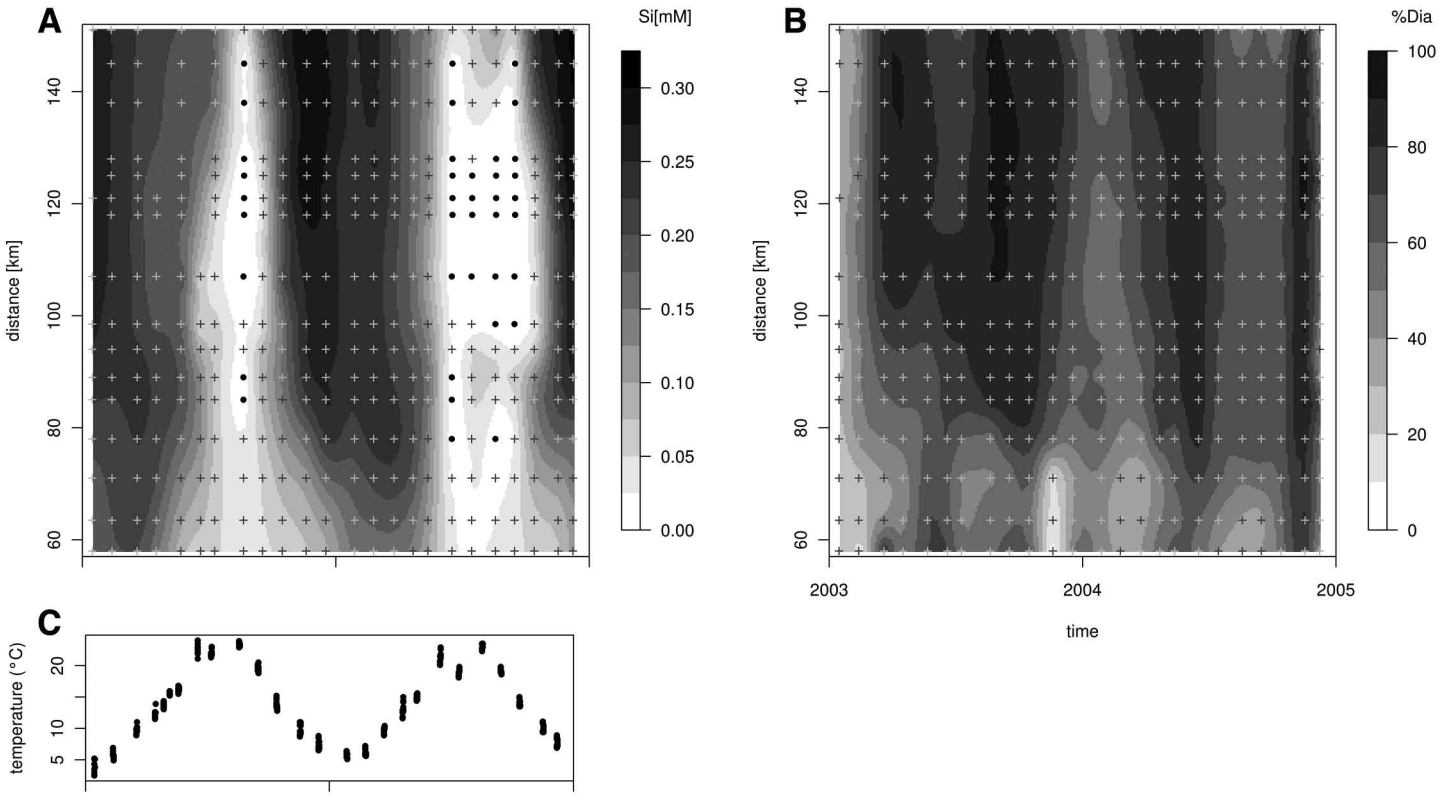

Fig. 2. Kriging interpolation plot of dissolved silica concentration (A), fraction of diatoms in the algal population (B), and seasonal variation of water temperature (C) as measured during the OMES measurement campaigns of 2003–2004. Individual samples are marked with gray +. Dissolved silica concentrations <10 µM, which can possibly indicate silica limitation of diatom growth, are marked with a black dot. Distance refers to kilometers from the mouth of the estuary.

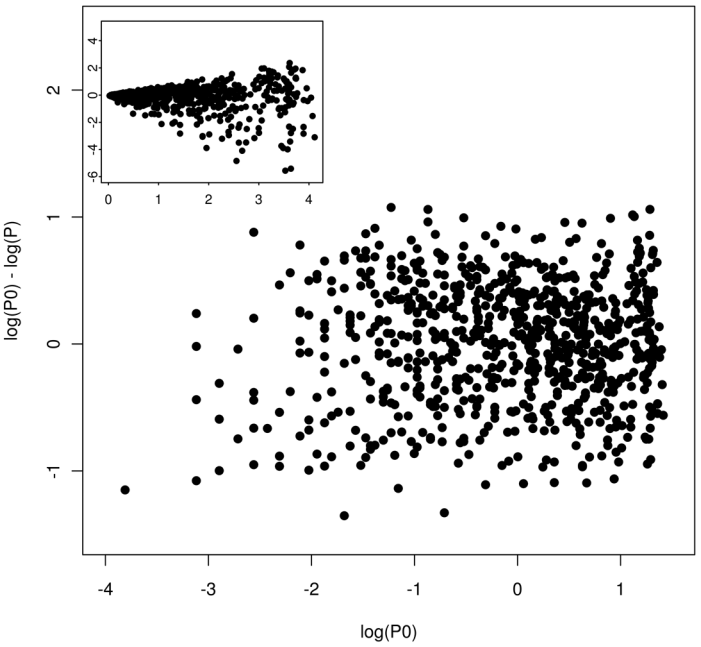

Fig. 3. Residuals versus the predicted values of the model *P*0. Untransformed (inset) and log-transformed (main figure).

phyll *a* determination was performed by fluorescence according to the procedure introduced by Yentsch and Menzel (1963), adapted by Strickland and Parsons (1972). Pigments were extracted with 90% acetone. A Shimadzu RF-1501 fluorometer was used for pigment analysis (excitation at 430 nm, emission at 670 nm). Correction for (and calculation of) phaeopigments was achieved by successive measurements before and after addition of 100 µL HCl (0.1 M). The procedure was calibrated by means of pure chl *a* extract (Sigma-Aldrich).

The CHEMTAX algorithm (Mackey et al. 1996) was used to distinguish between diatom and other algal groups' contribution to total chl *a*, using concentrations of accessory pigments. The initial pigment ratio matrix was based on published accessory pigment to chl *a* ratios in estuaries (Lewitus et al. 2005; Schlüter et al. 2000), as well as measured from cultures of major diatoms (*Cyclotella scaldensis* and *Stephanodiscus hantzschii*) isolated in the freshwater reaches of the Schelde estuary (Lionard et al. 2008). The relative contribution of diatoms to chl *a* in the FW tidal reaches varied between 22% and 97% (Fig. 2). The fraction of diatoms was highest in summer (on average 81% in 2003 and 73% in 2004) and lowest in winter (on average 47% in 2003 and 57% in 2004).

Statistical methods—Direct and two-step approaches: The starting point of the analysis of the P-I data is the Webb model (Webb et al. 1974), relating (algal) photosynthesis (*P*) to incident light intensity (*E*):

$$P0(\mathbf{x}_0, \boldsymbol{\theta}_0) = P_m \times \left(1 - \exp\frac{-\alpha.E}{P_m}\right) \quad (1)$$

in which the independent variable vector $\boldsymbol{x}_0 = [E]$ and the parameter vector $\boldsymbol{\theta}_0 = [\alpha, P_m]$; P_m is the maximum photosynthetic rate [gC (gChl . h)$^{-1}$], and α the photosynthetic efficiency [gC (gChl h)$^{-1}$/µmol photons (m^2 . s)$^{-1}$].

Classically, this model is fitted on individual observed photosynthesis-irradiance curves. When a collection of such data is available, the resulting set of parameters α and P_m can be used to study spatiotemporal variation of photosynthesis. We will call this the *two-step* approach. Usually, simple linear techniques (ANOVA, regression, principal components analysis [PCA]) are used to study the variation in the α and P_m estimates and their relation with abiotic factors (e.g., Kromkamp and Peene 1995; MacIntyre and Cullen 1996; Goebel and Kremer 2007). In contrast, we propose to extend the Webb model (Eq. 1), based on ecosystem-specific considerations regarding the factors that explain spatial and temporal patterns of photosynthesis. Among others, such factors could include temperature, nutrient availability, photo-acclimation, and changing phytoplankton species composition due to seasonal succession or selective grazing pressure. When we denote such an extended Webb model by $Pi(\boldsymbol{x}_i, \boldsymbol{\theta}_i)$, with $\mathbf{x}_i$ the vector of explanatory variables and $\boldsymbol{\theta}_i$ the parameter vector of this model, the corresponding models for α and P_m are given by

$$\alpha(\mathbf{x}_i, \boldsymbol{\theta}_i) = \left.\frac{dPi(\mathbf{x}_i, \boldsymbol{\theta}_i)}{dE}\right|_{E=0} \quad (2)$$

$$P_m(\mathbf{x}_i, \boldsymbol{\theta}_i) = \lim_{E \to \infty} Pi(\mathbf{x}_i, \boldsymbol{\theta}_i) \quad (3)$$

As such, the parameters of the extended Webb model can be estimated by fitting these models on the α and P_m determined in the first step. Note that the α and P_m equations have parameters in common. When fitted separately, the obtained parameter estimates will be specific for either α or P_m. Alternatively, a weighted least squares fit can be performed where one set of parameters is estimated based on the combined set of α and P_m values, weighted by their standard deviations. We will denote the two alternatives by *separate* and *joint* two-step fit, respectively.

The two-step approach above is close to the classic approach of analyzing sets of P-I data, and can be seen as an extension from linear to (well-chosen) nonlinear models relating photosynthesis to environmental factors. In addition we introduce the *direct* approach, in which extended Webb models $Pi(\mathbf{x}_i, \boldsymbol{\theta}_i)$ are fitted directly on the whole set of photosynthesis-irradiance points and environmental data, instead of first determining α and P_m from each P-I curve and then fitting the models 2 and 3.

Assessing model performance: Next we describe some statistical tools to assess the performance of the models used and the reliability of the parameter estimates obtained and their statistics, and to clarify the error structure of the models. We will particularly be dealing with sequences of nested models

$Pi(\mathbf{x}_i, \boldsymbol{\theta}_i)$ of increasing complexity. Two models are nested when the simplest of the two is derived from the more complex model by setting some of the latter's parameter values to a constant value, typically to eliminate certain terms or factors from the complex model. In such a case, the following test statistic can be used to check whether a data set supports the choice for the more complex model over the more simple one (Mizon 1977; Seber and Wild 1989). The (weighed) sum of squared residuals (SSR), taken as a measure for the goodness of fit, is compared successively between two models with a different number of parameters (a *full* and a *reduced* model, with degrees of freedom specified by df_f and df_r, the difference between the number of data points and the number of parameters). The following test statistic F is approximately distributed as $F_{df_r - df_f, df_r}$ when the reduced model describes the data set:

$$F = \frac{SSR_r - SSR_f}{SSR_r} \frac{df_r}{df_r - df_f} \approx F_{df_r - df_f, df_r} \tag{4}$$

We thus reject the reduced model at the δ level of significance when $F > F_{df_r - df_f, df_r}$ (Seber and Wild 1989). Application of these F tests on a sequence of models of increasing complexity can be seen as a selection scheme to assess which level of model complexity is supported by a given data set.

We use this F statistic first to test the fit of Webb's equation on each P-I curve against a linear P-I relation. As the maximal light intensity in the photosynthesis determination was chosen to reflect maximal in situ light intensity, the light to which the samples were exposed not always allowed for saturated algal growth, and P_m could not always be estimated. Second, the F statistic is used to test whether the more complex of a series of nested models, $Pi(\mathbf{x}_i, \boldsymbol{\theta}_i)$, or their derived α and P_m models, fits the data set significantly better than the more simple. When this is not the case, the parameters from the more complex model cannot reliably be estimated from the data set. This might be due to insufficient data, inappropriate model formulation or parameterization, or, specifically in our case, the fact that environmental variability included in the more complex model is not (significantly) influencing the photosynthetic rates.

Every inference on parameters $\boldsymbol{\theta}$ obtained by nonlinear regression assumes that the model $Pi(\mathbf{x}_i, \boldsymbol{\theta}_i)$ is correct, and that data points P are distributed around this model with either known or unknown properties of the distribution of the residual error term ε:

$$P = Pi(\mathbf{x}_i, \boldsymbol{\theta}_i) + \varepsilon \tag{5}$$

When prior information about the distribution of ε is available, we can straightforwardly apply a weighted least squares fitting method. As in most cases of nonlinear parameter estimation (Seber and Wild 1989), we do not have this information. In such a case, one has to resort to a nonweighted scheme, in which data and models are (iteratively) transformed until a structure is found in which (transformed) data are independent and identically distributed (i.i.d.) around the (transformed) model. The standard deviation of ε is approximated by $\hat{\sigma} = \sqrt{SSR / df}$, in which the residuals are calculated from the transformed model and data (Seber and Wild 1989). This error term quantifies the variation in the data that remain unexplained with the proposed model formulations, and is sometimes called *model uncertainty*. It originates from two main sources: (1) the models used are not complete—they constitute a simplified representation of reality and do not capture all mechanisms that control photosynthesis; (2) there always exists stochastic variability in the data set, as a result of natural variability and as the cumulative effect of (small) intrinsic errors in the measurement procedure. A failing Shapiro-Wilk test of the normality of the residuals can indicate that the model used does not account for specific events, giving rise to "more than normal" extreme values. It is generally impossible to attribute the noise term either to the model (1) or to the data (2); most commonly it is a combination of both.

Model uncertainty quantification is slightly different for the two-step procedure. After determining α and P_m from the individual P-I curves, the derived models (Eqs. 2 and 3) are fitted, from which error term statistics are obtained (as explained above). Modeled photosynthetic rates are obtained by substituting the α and P_m estimates, calculated by these models, in Webb's equation. Errors on modeled α and P_m induce errors on the estimate of photosynthetic rates. The statistics of this induced error term is determined with Monte Carlo methods: modeled α and P_m are perturbed (based on their respective error term statistics) and subsequently used to calculate photosynthetic rates, by substitution in the Webb model. By comparing the photosynthetic rates calculated by the perturbed and the nonperturbed model, we get an estimate of the induced error term.

Only when the residuals are normally distributed, the formal covariance matrix σ_{xy} (as calculated by algorithms of least squares optimization), can be set equal to the covariance matrix of the parameters (Press et al. 2003). This parameter covariance matrix provides an estimate of the *parameter uncertainty* (variance) and of their mutual dependence (covariance). A high estimated parameter variance indicates that the parameter cannot reliably be estimated from the data. A high cross-correlation (covariance) between two parameters indicates that they cannot be simultaneously estimated from the data set. The effect of parameter uncertainty on the model output, and its relative importance to the error term, can be assessed by means of Monte Carlo simulation, also allowing for a visualization of the stochastic parts of the model.

All analyses in this manuscript were performed in the R software for statistical computing (R Development Core Team 2006).

Specific model formulations for the study site: To apply the described method on the study site, we used the following set of nested models to take into account effects of seasonal vari-

ation, silica limitation, community composition, and spatial heterogeneity on community photosynthesis (formulations used will be discussed in "Assessment"). We first extend the model *P*0 (Eq. 1) to account for seasonal variation, modeled via a temperature dependence with a Q10-formulation:

$$P1(\mathbf{x}_1,\boldsymbol{\theta}_1) = P_{m,10} \times f(T) \times \left(1 - \exp\frac{-\alpha_{10}.E}{P_{m,10}}\right) \quad (6)$$

$$f(T) = Q_{10}^{\frac{T-10}{10}} \quad (7)$$

in which the independent variable vector now also includes temperature, i.e., $\mathbf{x}_1 = [E,T]$ and $\boldsymbol{\theta}_1 = [\alpha_{10}, P_{m,10}, Q_{10}]$; α_{10} and $P_{m,10}$ are now the maximal photosynthetic rate and the photosynthetic efficiency at the reference temperature of 10°C, and Q_{10} is the parameter determining the temperature dependence, i.e., the multiplication factor for a 10°C temperature increase.

Silica is the only nutrient potentially limiting algal growth in the study area. Nutrient limitation is taken into account by a multiplicative Monod formulation of the dissolved silica concentration ($\Lambda(DSi)$):

$$P2(\mathbf{x}_2,\boldsymbol{\theta}_2) = P_{m,10} \times f(T) \times \Lambda(DSi) \times \left(1 - \exp\frac{-\alpha_{10}.E}{P_{m,10}}\right) \quad (8)$$

$$\Lambda(DSi) = \frac{DSi}{DSi + k_{Si}} \quad (9)$$

in which $\mathbf{x}_2 = [E,T,DSi]$ and $\boldsymbol{\theta}_2 = [\alpha_{10}, P_{m,10}, Q_{10}, k_{Si}]$ and k_{Si} (mM) is the half-saturation constant of the Monod function.

As non-diatoms are not limited by dissolved silica concentrations, and periods in which a considerable fraction of the algal population consists of non-diatoms are observed, the model is further extended as

$$P3(\mathbf{x}_3,\boldsymbol{\theta}_3) = P_{m,10}^{dia} \times f^{dia}(T) \times \Lambda(DSi) \times \left(1 - \exp\frac{-\alpha_{10}^{dia}.E}{P_{m,10}^{dia}}\right) \times \frac{\%Dia}{100}$$
$$+ P_{m,10}^{n.dia} \times f^{n.dia}(T) \times \left(1 - \exp\frac{-\alpha_{10}^{n.dia}.E}{P_{m,10}^{dia}}\right) \times \left(1 - \frac{\%Dia}{100}\right) \quad (10)$$

with $\mathbf{x}_3$ = [*E*, *T*, *DSi*, %Dia] and $\boldsymbol{\theta}_3 = [\alpha_{10}^{\text{n.dia}}, \alpha_{10}^{\text{dia}}, P_{m,10}^{\text{n.dia}}, P_{m,10}^{\text{dia}}, Q_{10}^{\text{n.dia}}, Q_{10}^{\text{dia}}, k_{Si}]$, i.e., all parameters differ between diatoms (dia) and non-diatoms (n.dia).

Kromkamp and Peene (1995) observed quasilinear increasing P_m and α with increasing salinity. Because we are in particular interested in the parameter estimates in the freshwater tidal reach, we perform the nonlinear regression of the models *P*0–*P*3 first on the freshwater stations (salinity [*S*] ≤1 throughout the year). Next we multiply with an empirical linear relation of salinity, offset by the minimum observed salinity *min*(*S*), to test the correlation with salinity in the full data set. Thus every model *Pi* has a salinity-dependent variant *PiCl* = *f*(*S*)*Pi*, where $f(S) = 1 + b_S(S - min(S))$, to be applied on the combined freshwater and brackish water data set.

The associated models for α and P_m to be used in the two-step approach are derived straightforwardly (cf. Eqs. 2 and 3). Considering *P*2 as an example, taking the derivative with respect to *E* at *E* = 0 yields

$$\alpha^{obs,2} = \alpha_{10} \times f(T) \times \Lambda(DSi) = \Phi 2(\mathbf{x},\boldsymbol{\theta}^{\alpha}) \quad (11)$$

and the limit of *P*2 when $E \to \infty$ gives

$$P_m^{obs,2} = P_{m,10} \times f(T) \times \Lambda(DSi) = \Phi 2(\mathbf{x},\boldsymbol{\theta}^{Pm}) \quad (12)$$

in which $\mathbf{x} = [T, DSi]$, $\boldsymbol{\theta}^{\alpha} = [\alpha_{10}, Q_{10}{}^{\alpha}, k_{Si}{}^{\alpha}]$ and $\boldsymbol{\theta}^{Pm} = [P_{m,10}, Q_{10}{}^{Pm}, k_{Si}{}^{Pm}]$. Thus, these two equations represent the dependency of α and P_m on temperature and dissolved silica concentration in a way that is consistent with the model *P*2, and that correspondingly could be fitted to the α and P_m determined from each P-I curve. The models derived from *P*0–*P*3 will be denoted by Φ0–Φ3.

Note the parameters that the α and P_m equations have in common. In Φ2, for example: Q_{10} and k_{Si}. When fitted separately on the α and P_m values, the parameter estimates obtained will be specific for either α or P_m. Alternatively, a weighted least squares fit can be performed where one set of parameters is estimated based on the combined set of α and P_m values, weighted by their standard deviations. Such a *joint* fit is the counterpart of the direct fit procedure, leading to single values of the common parameters of the α and P_m equations.

Results and assessment

Comparison of direct, joint two-step, and separate two-step procedures—We applied the model selection and parameter estimation procedures to the P-I data set, gathered during 2003–2004 in the freshwater and brackish reaches of the Schelde estuary. The resulting parameter estimates (Tables 2 and 3) are discussed later in the article. We first present the results of the model selection procedure, the differences in results between the direct and the two-step procedures, and the quantification of model and parameter uncertainty.

First we examine the *direct fit* procedure. Inspired by the trumpet shape of the residuals-versus-predicted-values plot of the untransformed fit of *P*0, indicating a multiplicative error structure (Fig. 3), all model fits and sequential *F* tests were performed on log-transformed data and models to ensure a uniform variance.

The *F* tests indicated that all sequential extensions of the P-I model are supported by the freshwater data set at 0.001 significance level (Eq. 4). Standard *t* tests indicate the acceptance of all parameter estimates at the 0.001 level. The standard deviation $\hat{\sigma}$ of the error term decreases from 0.47 in *P*0 to 0.39 in *P*3. Back-transformed from the log-transformed models, this means a decrease of 20% of the relative error bound

Table 2. Results of the parameter fits of the models *P*0–*P*3Cl.

	*P*0	*P*1	*P*2	*P*3	*P*3Cl
α^{dia}	0.0111 (0.0003)	0.0101 (0.0003)	0.0099 (0.0003)	0.0119 (0.0004)	0.0115 (0.0004)
$\alpha^{n.dia}$	—	—	—	0.0030 (0.0009)	0.0068 (0.0006)
P_m^{dia}	6.6 (1.1)	6.0 (0.9)	5.4 (0.6)	5.1 (0.5)	5.6 (0.5)
$P_m^{n.dia}$	—	—	—	5.1 (0.5)	5.6 (0.5)
Q_{10}^{dia}	—	1.16 (0.04)	1.54 (0.05)	1.48 (0.07)	1.55 (0.07)
$Q_{10}^{n.dia}$	—	—	—	3.7 (0.8)	1.9 (0.2)
k_{Si}	—	—	0.0018 (0.0002)	0.0044 (0.0006)	0.0046 (0.0005)
b_S	—	—	—	—	0.091 (0.007)
$\hat{\sigma}$ (df)	0.473 (774)	0.468 (773)	0.407 (772)	0.386 (770)	0.399 (1197)

Parameter values are presented with standard deviation in parentheses. Estimates and statistics are calculated for the log-transformed version of the models *P*0–*P*3Cl, as is the estimated standard deviation $\hat{\sigma}$ of the error term ε; only freshwater data ($S < 1$) is used for *P*0–*P*3; all data are used for *P*3Cl. The exact interpretation of the parameters is dependent on the formula, e.g., the presented α^{dia} is the value at 10°C for *P*1, whereas it represents an average value at all temperatures for *P*0. All model extensions are supported by the data set. See text for further information. Units: α, gC (gChl . h)$^{-1}$/μmol photons (m^2 . s)$^{-1}$; P_m, gC (gChl . h)$^{-1}$; k_{Si}, mM; b_S, (–).

Table 3. Results of two-step parameter fits and model selection scheme.

	Separate fit		Joint fit
	Φ2Cl$^{\alpha}$	Φ2Cl^{Pm}	Φ2Cl
α_{10}	0.0129 (0.0009)	—	0.0127 (0.0008)
$P_{m,10}$	—	4.8 (1.0)	4.8 (0.4)
Q_{10}	1.5 (0.1)	2.8 (0.5)	1.8 (0.1)
k_{Si}	0.007 (0.003)	0.06 (0.05)	0.015 (0.005)
b_S	0.08 (0.01)	0.09 (0.04)	0.08 (0.01)
$\hat{\sigma}$ (df)	0.0073 (147)	3.3 (62)	0.74 (212)

Parameter estimates are shown for the models that were selected by the *F* test nested model scheme on the total data set. Units as in Table 2.

(*exp(± $\hat{\sigma}$)) on the photosynthetic rate, from [–38%, +60%] to [–32%, +46%]. Only the residuals of the (selected) model *P*3 are normally distributed (Shapiro Wilk: $W = 0.998$, $P = 0.54$), which confirms that the models *P*0–*P*2 miss specific events (seasonality by *P*0, silica limitation by *P*0–*P*1, non-diatom takeover by *P*0–*P*2), giving rise to a non-normal distribution of the residuals.

Similarly, when fitted on the total data set (freshwater and brackish reaches), the choice for the most complex model (*P*3Cl) is supported by the sequential *F* tests, and standard *t* tests indicate acceptance of the parameter estimates at the 0.001 level. Because the brackish reaches show higher relative abundance of non-diatoms, the salinity-dependent model not only sheds light on spatial heterogeneity of the photosynthetic parameters, but also reduces non-diatom parameter uncertainty. The estimated parameter covariances $\hat{\sigma}_{xy}$ reveal that $\alpha^{n.dia}$ and $Q_{10}^{n.dia}$ are highly negatively correlated when fitted on only the freshwater data ($\hat{\sigma}_{xy} = -0.94$), indicating that the simultaneous estimation of these two parameters is impossible from the freshwater data set only. This negative correlation is considerably reduced when *P*3Cl is fitted on the whole data set (Fig. 4), although it is still the highest cross-correlation in the parameter estimates ($\hat{\sigma}_{xy} = -0.67$). The second highest cross-correlation in *P*3Cl is observed between α^{dia} and Q_{10}^{dia} ($\hat{\sigma}_{xy} = -0.58$), but this is less important given the lower uncertainty of these parameters (cf. standard deviations in Table 2). Estimates of the other parameters (P_m, k_{Si}, b_S) display overall low cross-correlations. This suggests that, except for the non-diatom parameters, all parameters of the models *P*0–*P*3 and *P*0Cl–*P*3Cl can be estimated from the data set.

The results of the model selection scheme performed on the *two-step* fits (the search for seasonality, spatial variability, and effects of silica depletion and community composition on photosynthetic parameters) are more ambiguous. First, due to the measurement procedure only for 66 of the 151 observed P-I curves, it was possible to estimate a P_m value; the others were rejected based on the comparison of the fit of Webb's equation with a linear P-I relation (*F* test, 0.01 level). In the *separate* two-step procedure, the estimates of the parameters Q_{10}, k_{Si}, and b_S are allowed to be different for α and P_m. When fitted on the α and P_m values determined from the individual P-I curves, the *F* tests indicate the preference of the models Φ2 (Φ2Cl), incorporating temperature dependence and silica limitation, for both the freshwater and the total data set. However, while parameter estimates for α seem acceptable, with only k_{Si} accepted with a lower power ($P = 0.01$ when fitted on the freshwater data set and $P = 0.05$ when fitted on the total data set), this is not the case for P_m. For the freshwater subset, both P_m^{dia} and k_{Si} estimates are rejected ($P > 0.6$). When fitted on the total data set, the estimate of P_m^{dia} is accepted at the 0.001 level, but the estimate for k_{Si} is still rejected ($P > 0.18$). This leaves us with the conclusion that there is clearly an effect of seasonality and silica limitation for both α and P_m, but that parameter estimates for relations describing the effect of silica limitation on P_m data are unreliable. Parameter estimates are presented in Table 3.

When the models Φ0–Φ3 are fitted using a *joint*, weighted fit of the α and P_m data, only one set of the parameters k_{Si}, Q_{10}, and

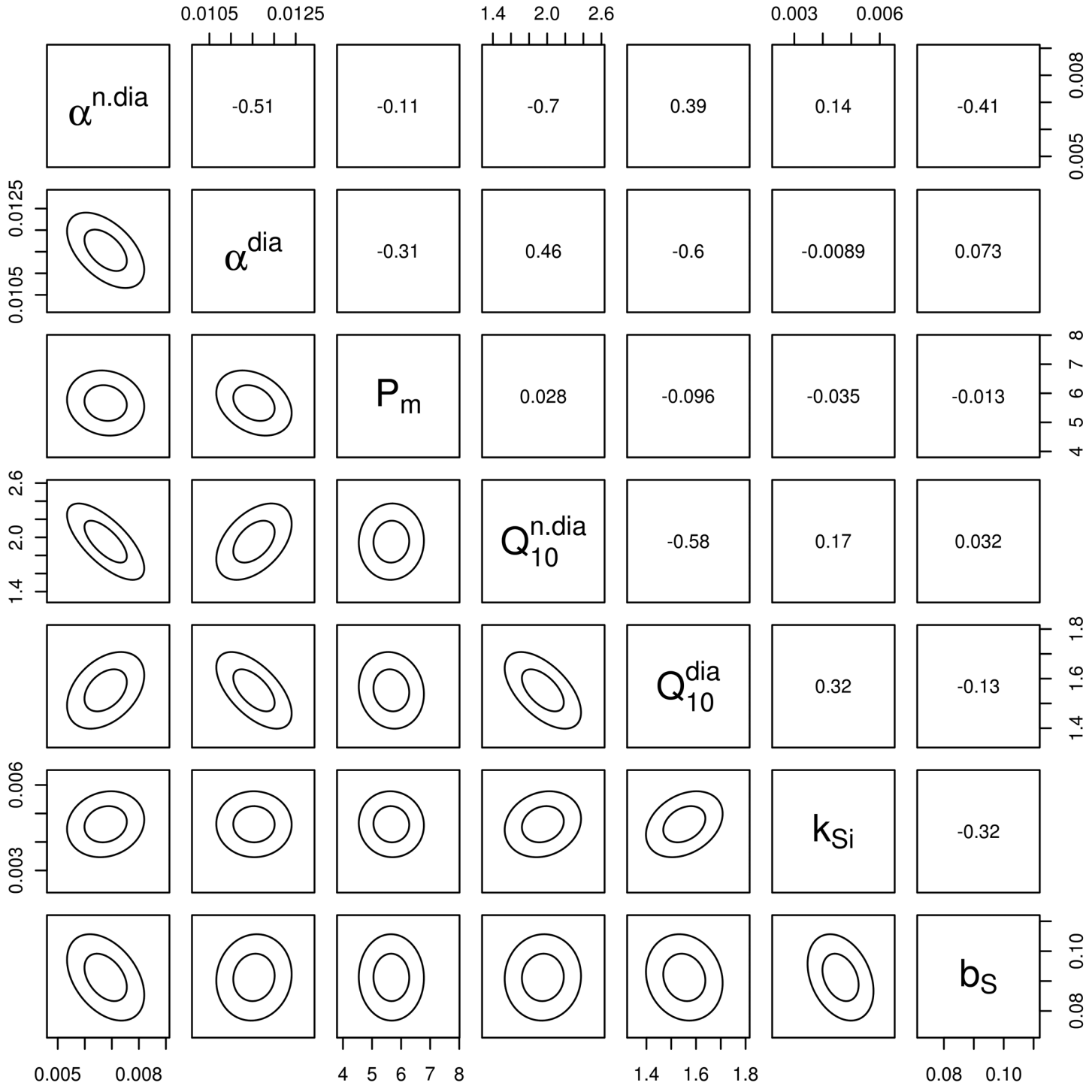

Fig. 4. Estimated covariance matrix of the parameters of the model *P*3Cl, visualized by plotting the 50% and 90% ellipses of all parameter combinations (lower left part). The correlation coefficient of each parameter combination is given in the upper right part.

b_S and is obtained. In this selection scheme, the model Φ3 is selected when fitted on the freshwater subset, but only Φ2Cl when fitted on the total data set. Standard *t* tests indicate acceptance of all parameter estimates at the 0.001 level except for k_{Si}; the estimate of k_{Si} is accepted at the 0.01 level when estimated from the total data set, but is rejected when Φ3 is fitted on the freshwater data set. The obtained parameter estimates are largely comparable to the estimates of the *direct* fit, except for the estimate of k_{Si}, which is larger in the two-step fit by a factor of 3. For all parameters, both the variances and cross-cor-

relations are much higher in the two-step fit procedure. In particular, the estimates of k_{Si} and Q_{10} are highly correlated ($\hat{\sigma}_{xy}$ = –0.53), and both parameters cannot be estimated simultaneously from this data set. Both deviate from the direct fit estimates by twice their standard deviation, indicating that this cross-correlation is the cause of the unrealistic parameter estimate of k_{Si}, and to a lesser extend Q_{10} in the two-step approach. The failure to select the most complex model Φ3 (in both the separate and the joint fits) would suggest no effect of community composition (diatoms versus non-diatoms) on the photosynthetic parameters. The acceptance of Φ3 when fitted only on the freshwater subset does hint at a possible effect of community composition, but the concomitant rejection of the estimate of k_{Si} makes this assertion uncertain.

The direct and two-step procedures are further compared in two ways, namely by their capability to reproduce spatiotemporal patterns of the photosynthetic parameters on the one hand, and their capability to reproduce observed photosynthetic rates on the other. The spatial and temporal patterns of the photosynthetic efficiency α and the correspondence with the selected models are presented in Figs. 5 and 6. For the direct fit, the derived formulations from *P*3Cl are used (i.e., Φ3Cl, similar to Eq. 11), with parameter values obtained in the direct fit (Table 2). The photosynthetic efficiency (and the corresponding models) shows a distinct overall spatiotemporal pattern, with a clear seasonality, interfered by the effects of silica limitation and with a downstream increasing trend superimposed on it. The effect of silica depletion is reflected by the extremely low α values in summer. In 2003, depletion was recorded during a single month (August) at several stations in the freshwater reach (Fig. 2), giving rise to a pronounced minimum in the α values (Fig. 5). In 2004, the extended period of silica depletion (Fig. 2) gave rise to overall lower α, compared with 2003 (Fig. 5). Silica depletion also increases the variation of the photosynthetic efficiency along the salinity gradient: the increase with salinity is most pronounced when it is complemented with silica depletion in the freshwater reach. Most striking is the factor-4 difference between maximum and minimum photosynthetic efficiency in August 2003 and 2004 along the estuary axis, correctly reproduced by the models (Fig. 6). The 66 withheld P_m values result in a sparse data set. Therefore, the correspondence between observed and modeled spatiotemporal patterns of P_m is not very instructive, and is not shown. By construction, however, the modeled P_m displays the same spatiotemporal features as α (in the case of the joint fit the modeled P_m is proportional to the modeled α).

Although the model selection scheme and the overall reproduction of spatiotemporal patterns demonstrate relevance of the models used and the parameter estimates, regression of the modeled α and P_m against the respective values determined from the individual P-I curves shows considerable scatter (Fig. 7 B and C). This illustrates that a lot of variability in the parameters remains unexplained by the models, likely owing to the simplicity of the formulations, and partly to natural variability and introduced measurement errors.

In the end, we are not interested in photosynthetic parameters only, but also in (the accuracy of) the estimate of photosynthetic rates. In case of the two-step fits, photosynthetic rates are calculated by substituting the modeled α and P_m in Webb's equation. This results in a new selection scheme for the two-step fits, now based on the residuals of the photosynthetic rates. As can be read from Table 4, the models selected in the two-step scheme underperform when used to calculate photosynthetic rates. The residual error of the selected model is larger than for the simplest model in the direct fit (*P*0, i.e., one curve fitted through all P-I data points; Table 2), and the residuals of this selected model are larger than the ones from the more simple models. As such, while based on the α and P_m values the models Φ2Cl are selected, they would be rejected based on the photosynthetic rate data. In the new selection scheme, the model Φ1Cl would be preferred for the joint two-step fits, whereas Φ3Cl for α in combination with Φ1Cl for P_m would be preferred for the separate two-step fits (*F* test, 0.01 level).

Thus, although there is certainly spatiotemporal variation in the photosynthetic parameters that is partly reproduced by the respective models (cf. Figs. 5 and 6), these formulations and associated parameter estimates underperform when used to calculate photosynthetic rates. This reflects the changing *shape* of the P-I curve under, e.g., silica-depleted conditions: only a Webb-shaped P-I curve is entirely characterized by the initial slope and the maximal value of this function.

Moreover, when only studying the photosynthetic parameters, the above comparison of calculated and observed photosynthetic rates is normally not possible, as the original P-I data are needed. The *induced* residual error, calculated by Monte Carlo simulation based on the residual error of the α and P_m model fits (Table 3), is distinctly larger than the real residual error, for both the separate and the joint procedure (Table 4). These results suggest that the two-step procedures, as they are applied on fewer data points, result in an underestimation of the (already poor) predictive capacity of the fitted models when used to calculate photosynthetic rates.

Finally, a Monte Carlo simulation also sheds light on the relative importance of parameter uncertainty and residual uncertainty. Random parameter values $\tilde{\theta}$ are calculated based on the estimated covariance matrix. The effect of parameter uncertainty on the calculated photosynthetic rates is only 8% of total uncertainty (perturbed parameters + residual error) in the direct fit (Table 4), demonstrating that model uncertainty (the residual error term) is the main contributor to uncertainty in photosynthetic rate calculations, even with the model *P*3Cl (Fig. 8). In the two-step fit procedure, the estimated contribution of parameter uncertainty is higher, but still relatively small compared with total uncertainty (Table 4).

Assessment of parameter estimates and model formulations—As a first step in the two-step fit procedure, α and P_m values are obtained from each P-I curve. Freshwater α values are in the

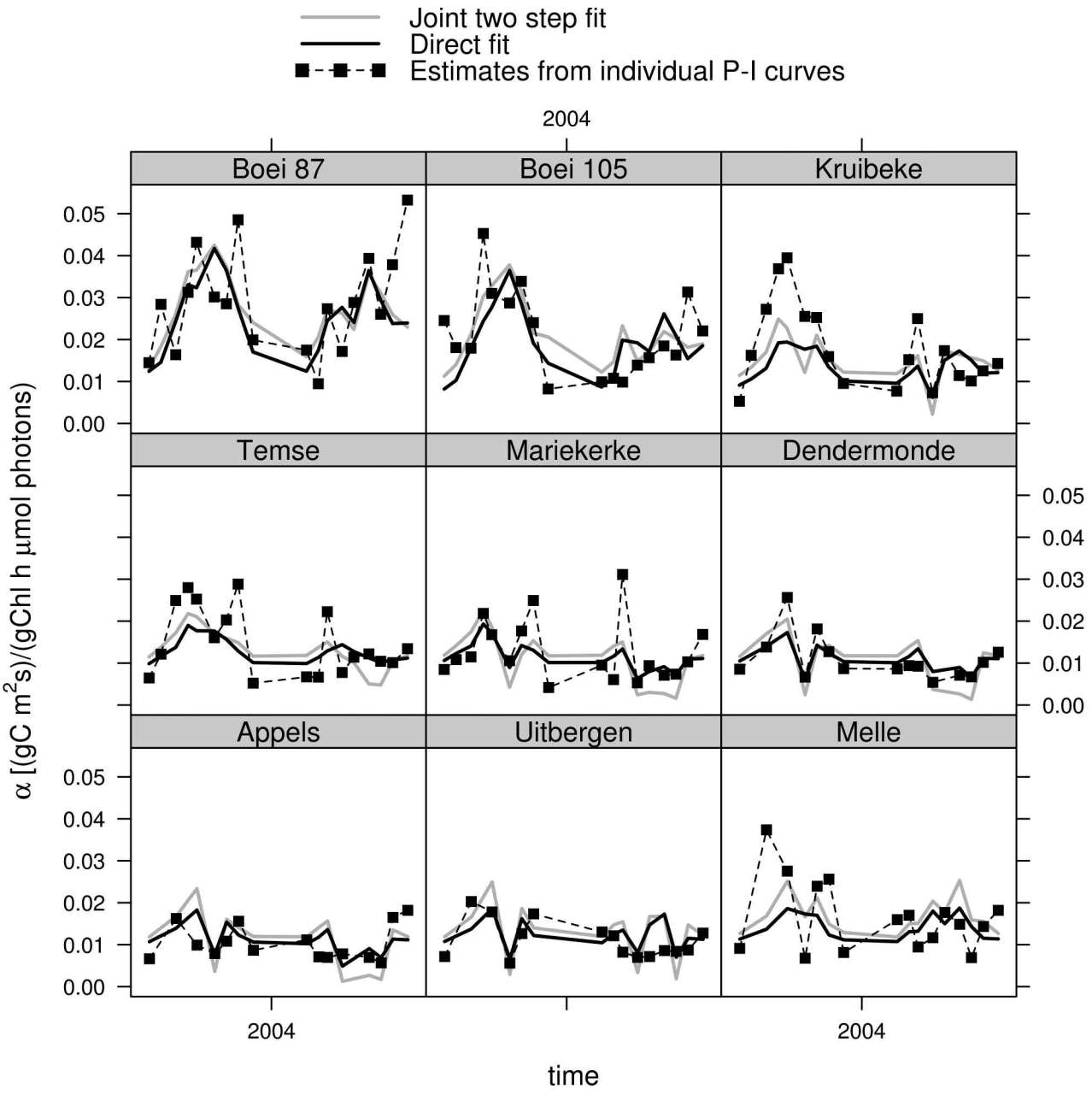

Fig. 5. Photosynthetic efficiency α versus time for the different monitoring stations. Points represent α values estimated from individual P-I curves. Lines represent modeled values, calculated with formula Φ3Cl and with the corresponding parameter values from the direct fit and the joint two-step fit (Tables 2 and 3). Observed and modeled photosynthetic efficiency display a clear seasonality interrupted with low values resulting from silica limitation.

range 0.004–0.037 gC (gChl . h)$^{-1}$/µmol photons (m^2 . s)$^{-1}$. Kromkamp and Peene (1995) report α values at the downstream part of the freshwater reach of 0.005–0.08 gC (gChl . h)$^{-1}$/µmol photons (m^2 . s)$^{-1}$. The average value we obtain is lower than in this study, 0.013 versus 0.032 gC (gChl . h)$^{-1}$/µmol photons (m^2 . s)$^{-1}$. Freshwater P_m values are in the range 1.10–18.4 gC (gChl . h)$^{-1}$, consistent with reported values of 0.7–18.8 gC (gChl . h)$^{-1}$ at the most downstream part of the freshwater reach (Kromkamp and Peene 1995). Also here, average values are lower, 4.4 versus 8.0 gC (gChl . h)$^{-1}$. As our samples were taken in the freshwater reach, while the data from Kromkamp and Peene (1995) are from the downstream boundary, this is consistent with the already observed decreasing trend of α and P_m along the salinity gradient (Kromkamp and Peene, 1995).

Both the direct and the two-step approaches result in estimates of model parameters. For a correct interpretation of these estimates, we need to realize that P-I curves reflect obser-

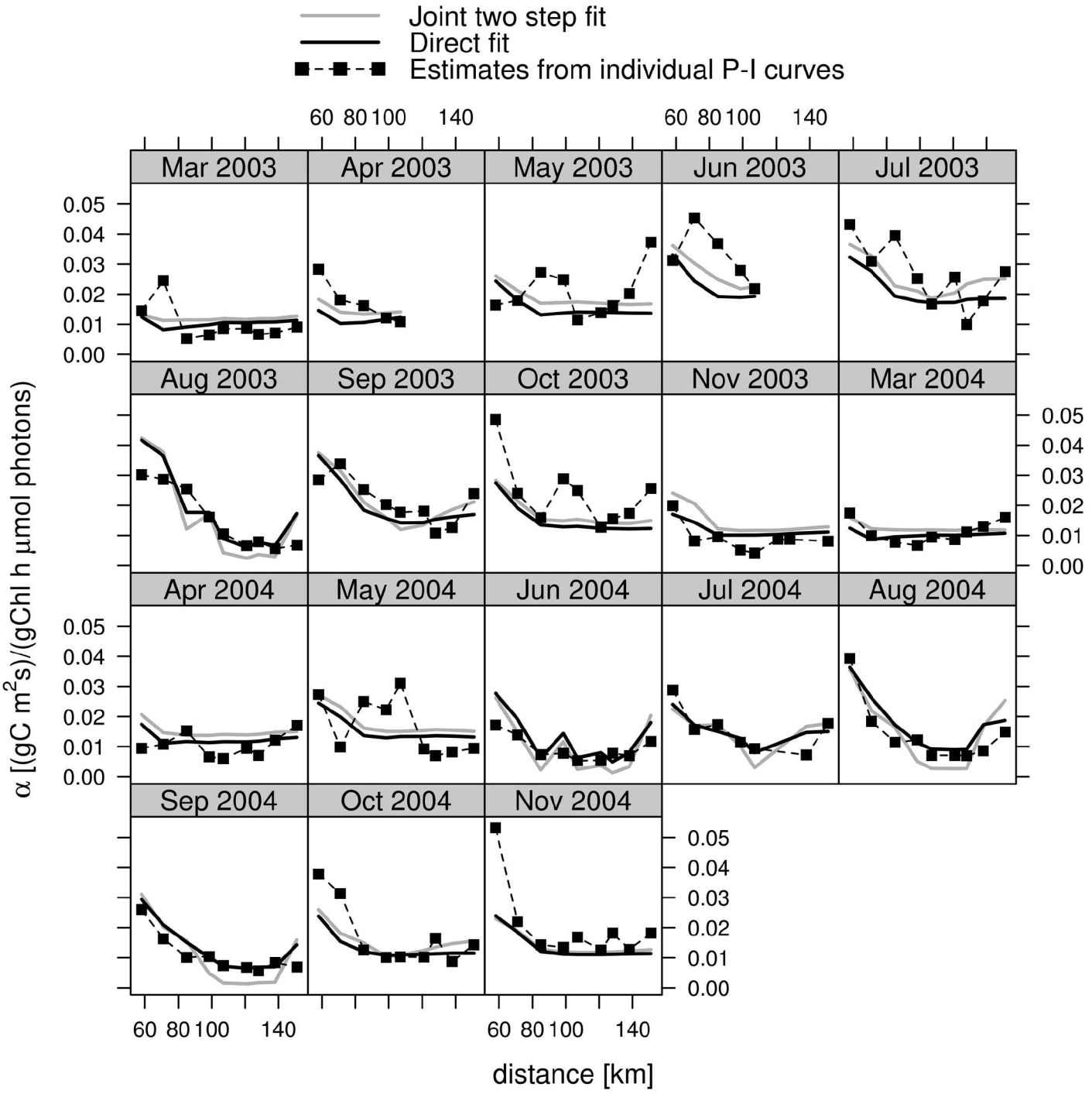

Fig. 6. Photosynthetic efficiency α versus distance from the estuary mouth for the different months of sampling. Points represent α values estimated from individual P-I curves. Lines represent modeled values, calculated with formula Φ3Cl and with the corresponding parameter values from the direct fit and the joint two-step fit (Tables 2 and 3). Observed and modeled photosynthetic efficiency display a clear downstream increasing trend, becoming more pronounced when silica is depleted in the freshwater reaches.

vations of photosynthesis of a varying phytoplankton community. Therefore, although the model structure is mathematically similar to simple models of single-species photosynthesis, both model output and parameter estimates should be interpreted in terms of community photosynthesis. This is the major difference with other model studies. In particular, Geider et al. (1997) used very similar models, but applied them to single-species data. Specifically, the observed seasonality is the

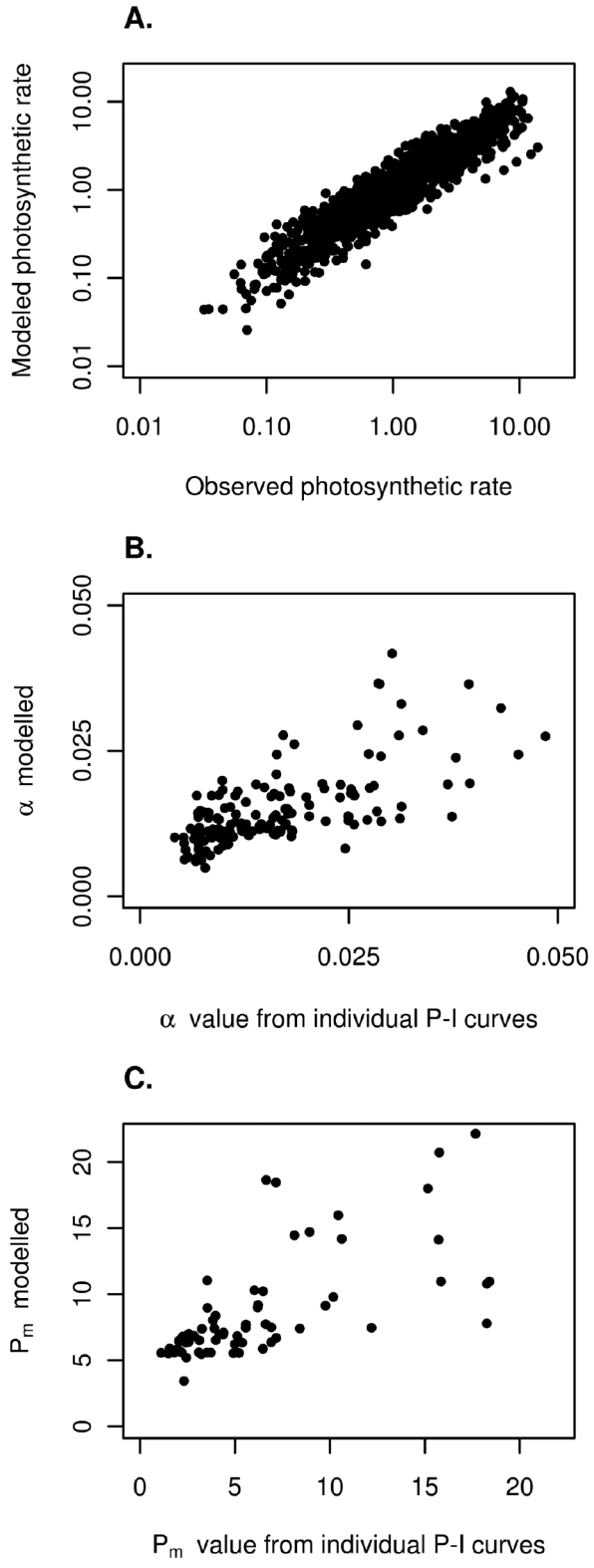

Fig. 7. Photosynthetic rates calculated with the directly fitted model (*P*3Cl) versus observed rates (A; note the log scale). Modeled photosynthetic efficiency (B) and maximum photosynthetic rate (C), calculated with parameter values from the direct fit, versus respective values from individual P-I curve fits.

aggregated result of the succession of phytoplankton species (with associated photosynthetic characteristics) and effects of temperature on photosynthetic rates. Therefore, the estimated Q_{10} parameter is conceptually different from the ones obtained from single-species studies, which represent only effect of temperature on photosynthesis. Similar remarks can be made about the estimated k_{Si}.

This also implies that insights from single-species studies on model structure or physiology should be carefully examined on their meaning and relevance for community photosynthesis. For instance, there is little temperature dependence of photosynthetic efficiency of individual species (Coles and Jones 2000; Morris and Kromkamp 2003). But this does not mean a priori that a multiplicative temperature dependence of community photosynthesis (as used above) is inappropriate. On the contrary, the results from our analysis demonstrates that there is seasonal variability in the α of the community photosynthesis.

Concerning the effect of nutrient limitation on community photosynthesis, the argument is slightly different. There is empirical evidence that the effect of nitrogen depletion on single-species algal growth is not best described by a multiplicative factor (Flynn 2003a), and this should also hold for community photosynthesis. However, Lippemeier et al. (1999) observed a direct effect of silica limitation on the photosynthetic performance of diatoms and assumed a strong influence of silicate metabolism on the photosynthetic efficiency. This supports the choice for a model formulation in which low silica concentrations affect not only P_m but also α. Our analysis confirms this observation, specifically by the selection of the model Φ2 for α in the two-step fit procedure. Lower values of α during periods of silica depletion are also obvious in Figs. 5 and 6.

Finally, the parameter covariance, as presented in Fig. 4, should also not be interpreted as if these parameters necessarily would co-vary; rather, it indicates whether the different parameters can be estimated independently in this model fit scheme. A high correlation between two parameters indicates this is not the case.

The foregoing remarks notwithstanding, the parameter estimates obtained in the direct fit are realistic, in the sense that they are comparable to literature values of their physiological counterparts. Sobrino and Neale (2007) reported a Q_{10} value of 1.4 for the growth of the estuarine diatom *Thalassiosira pseudonana* over the temperature range 10–20°C, which is close to the Q_{10} value from the direct fit (1.48 in freshwater, 1.55 for the total data set; Table 2). The half-saturation for silica limitation (k_{Si}) of 4.5 µM is at the higher end of reported half-saturation values for diatom growth, with these highest values reported specifically for growth in freshwater environment (Martin-Jezequel et al. 2000). So, although care has to be taken with the interpretation of parameters, their numerical values are confined by their physiological counterparts. This gives extra support for the nested model procedure.

Table 4. Residual standard deviation of calculated photosynthetic rates ($\hat{\sigma}$), induced residual standard deviation for the two step procedures calculated with Monte Carlo simulation ($\hat{\sigma}_{ind}$), and parameter uncertainty ($\hat{\sigma}^{par}$) calculated with Monte Carlo parameter perturbation based on the estimated parameter covariance matrix.

	$\hat{\sigma}$	$\hat{\sigma}_{ind}$	$\hat{\sigma}^{par}$
Direct fit			
*P*3Cl	0.40	—	0.032
Joint two-step fit			
Φ1Cl	0.47		
Φ2Cl	0.59	0.69	0.12
Φ3Cl	0.45		
Separate two-step fit			
$\Phi 2Cl^{\alpha} + \Phi 1Cl^{Pm}$	0.46		
$\Phi 2Cl^{\alpha} + \Phi 2Cl^{Pm}$	0.59	0.71	0.16
$\Phi 2Cl^{\alpha} + \Phi 3Cl^{Pm}$	0.47		
$\Phi 3Cl^{\alpha} + \Phi 1Cl^{Pm}$	0.43		

Values corresponding to the selected models in the two-step procedure are italicized.

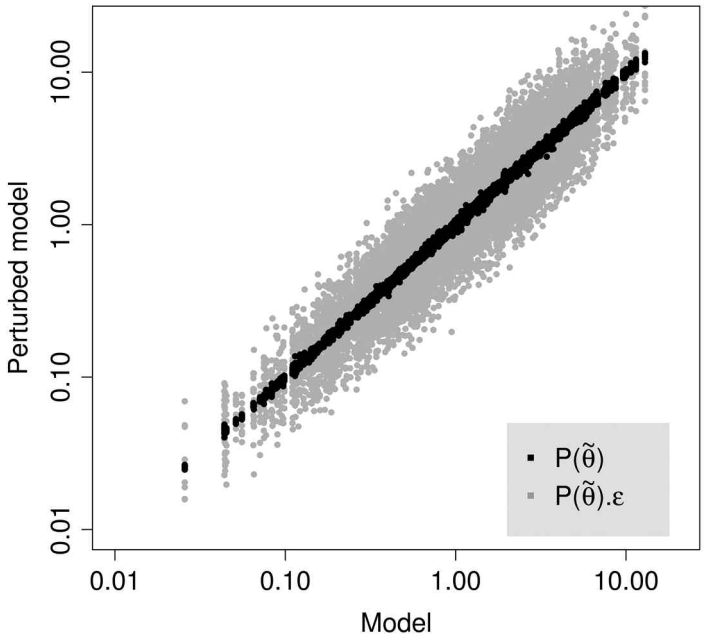

Fig. 8. Modeled photosynthetic rates and perturbed model results for the direct fit (model *P*3Cl). Black dots represent calculated photosynthetic rates with perturbed parameter estimates (Monte Carlo calculation based on the estimated covariances). Gray dots represent Monte Carlo calculations with perturbed parameter estimates and an additional random error term based on the estimated residual variance.

Discussion

The procedures introduced allow for a model-driven analysis of sets of P-I data to investigate variability in photosynthesis-irradiance curves. First, they can be used as a data analysis tool, to assess whether observed spatial or temporal trends in photosynthesis data can be ascribed to known factors and to what extent. In the example case of the Schelde estuary, we could demonstrate that seasonality, silica depletion, and phytoplankton community composition have effects on photosynthesis that are reflected in the observed P-I curves, and that are partly predictable. In contrast to classical analysis of photosynthetic parameters, where linear response functions are often assumed (ANOVA, PCA, linear regression), the explicit use of models forces one to propose appropriate functional relations. Second, we showed that the introduced approach can be used for parameter estimation of photosynthesis models. P-I data are obtained from in situ phytoplankton populations, thus circumventing some of the disadvantages of scaling up results from single-species studies to the ecosystem scale. This requires careful interpretation of the results, however, as insight derived from single-species studies cannot straightforwardly be extrapolated to community photosynthesis. This also has implications for the choice of model formulations. These considerations were discussed extensively in "Parameter assessment."

Direct versus two-step procedure—The choice for a direct or a two-step procedure partly depends on the aim of the study: as the photosynthetic efficiency α and the maximal photosynthetic rate P_m are determined by different physiological processes (respectively light harvesting and the Calvin cycle), it is perfectly legitimate to study the two parameters separately. However, we demonstrated that when the aim is to use these parameters for the calculations of photosynthetic rates, the two-step procedure seems inferior: the residual error on photosynthetic rates, calculated with the selected models Φ2 for α and P_m, is larger than the residual error of the simplest possible model *P*0, i.e., fitting one PE curve through all P-I data points. Also, because of the relatively few accepted P_m values in the freshwater reach, we could not conclude that there is an effect of silica limitation on P_m in the freshwater reach. An additional effect of community composition was not found for either α or P_m.

An essential part of the fitting procedure is the variance estimate of the residual error term in Eq. 5, accounting for the unexplained variability in the photosynthesis estimates. We observed that the residual variance is by far the most important source of uncertainty when calculating photosynthesis with the models used (Fig. 8). It is impossible to ascribe the residual variance to the inadequacy of the used models, to natural variability in the system or the method, or to the cumulative effect of (small) measurement errors. But obviously part of the residual variance results from the rather simple model formulations. When these models are used to calculate photosynthetic rates, the effect of this error term can be taken into account with Monte Carlo simulation.

It is clear that when the aim is to retrieve reliable models and associated parameter estimates to calculate photosyn-

thetic rates, the direct fit approach is more appropriate. Moreover, the parameter estimates obtained from the analysis of P-I curves might be more useful for ecosystem models than parameter values from single-species studies. For example, concerning the Q_{10} values, in these models it is exactly the seasonality (i.e., the aggregate effect of successive phytoplankton populations and the temperature dependence of photosynthetic rates) that has to be reproduced, and not specifically the temperature dependence of photosynthesis.

Of course the usual precautions need to be taken when using these parameter estimates for model studies outside the study period for which parameters are estimated. Particularly for our study site, considerable changes in phytoplankton biomass and species composition have been reported over the last decade (Cox et al. 2009). Possibly these changes also affected the community photosynthesis parameters, their seasonal variation, and their responses to nutrient limitation. In such a setting, the parameter estimates and model formulations can be considered valid only for the study period, unless an additional validation study is performed with other data. Besides, in such a validation study the presented method could prove to be a useful tool. When a new data set would be available for validation, the methods outlined above could be used to assess whether a model with data set–specific photosynthesis parameters fits the data significantly better than a model with constant parameters for the combined data set. Otherwise, when applying the models and parameter estimates in model simulations for the 2003–2004 period, it is clear that the parameters as presented give the best "average" model output for the period. Moreover, parameter estimates from the direct fit on the 2003 data only are very similar to the estimates obtained in the fit from 2003–2004. On the other hand, in 2004 the prolonged period of silica limitation almost completely masks the seasonality (Fig. 5). When models are fitted on this subset, the parameter estimates are unphysical, notably with a Q_{10} value smaller than 1. This illustrates a general weakness of the presented method compared with laboratory studies. When different environmental factors interact and potentially neutralize each other, success of the method presented will partly depend on the access to a good data set, where the effect of the different factors is separable.

Extension to more complex models—Although the model structures we used are fairly standard and widely used (Webb model for photosynthetic rate, Monod formulation for silica limitation, Q_{10} structure for temperature dependence), they are empirical mathematical formulations for algal growth and photosynthesis for which more detailed mechanistic models have been developed (Flynn 2003b; Baklouti et al. 2006). It is possible to generalize the method outlined and fit more complex models to measured P-I curves. It has been reported that published data sets (mainly based on laboratory cultures) are not adequate for rigorous testing of complex models (Flynn and Martin-Jezequel 2000), a statement that was made in the context of the interaction between silica stress and photosynthesis. Our study suggests that elaborate sets of (in situ) measured P-I curves, and to a lesser extent sets of α and P_m values determined from individual P-I curves, under varying environmental conditions, could be valuable data sets for the evaluation of these complex models. Because they aim at a broad applicability, they should at least be able to reproduce these curves and the photosynthetic parameters α and P_m.

Comments and recommendations

Fitting models to historical and present P-I data provides a useful tool to study the role of certain environmental cues on variation in phytoplankton community photosynthesis. In contrast to results from laboratory and single-species studies, sets of P-I data reflect the behavior of natural phytoplankton assemblages. The model-based study of these P-I data provides insight to the relation between the variability in community photosynthesis and environmental covariates. Such study complements single-species studies, from which it is not straightforward to infer characteristics of phytoplankton assemblages at the ecosystem scale. The parameter estimates that can be retrieved from the study of P-I data might be more useful in ecosystem models than literature values from single species.

Strikingly, there is a large amount of residual variation not accounted for by the used model formulations. Obviously, this partly results from the simplicity of the model formulations used, although they are common in ecosystem models. But also, species composition in the study area is considerably dynamic, and it would be interesting to investigate in more detail the effect of phytoplankton species succession on assemblage photosynthesis. This could also shed light on the accurateness of ^{14}C incubation to estimate community photosynthesis. Information on the origins of variability of community photosynthesis is important to assess the year-to-year variability and predictability of ecosystem photosynthesis.

To prevent overfitting of multiparameter models, we have put forward some statistical tools based on a nested model selection scheme. Refinement of these tools is probably possible. The quality of the results depend on the quality of the variety of data sources used (^{14}C incubations, nutrient concentrations, species composition determination). Therefore, the assessment of the resulting parameter estimates and the evaluation of the model formulation used will benefit from the use of more advanced statistics. Probably, also these statistics will need to be adapted to the specific situation when applied to other systems.

We conclude that a direct fit is to be preferred when the aim is to characterize and reproduce the variability of photosynthetic rates. The use of P-I data allows for a more powerful analysis of community photosynthesis. Therefore it is recommended that not only photosynthetic parameters are documented and analyzed, but rather the whole set of P-I data.

References

Alpine, A. E., and J. E. Cloern. (1988). Phytoplankton growth-rates in a light-limited environment, San-Francisco Bay. Mar Ecol-Prog Ser. 44:167–173. [doi:10.3354/meps044167].

Baklouti, M., F. Diaz, C. Pinazo, V. Faure, and B. Queguiner. (2006). Investigation of mechanistic formulations depicting phytoplankton dynamics for models of marine pelagic ecosystems and description of a new model. Prog. Oceanogr. 71:1–33. [doi:10.1016/j.pocean.2006.05.002].

Cole, B. E. (1989). Temporal and spatial patterns of phytoplankton production in Tomales bay, California, USA. Estuar. Coast. Shelf Sci. 28:103–115. [doi:10.1016/0272-7714(89)90045-0].

Coles, J., and R. Jones. (2000). Effect of temperature on photosynthesis-light response and growth of four phytoplankton species isolated from a tidal freshwater river. J. Phycol. 36:7–16. [doi:10.1046/j.1529-8817.2000.98219.x].

Cox, T. J. S., T. Maris, K. Soetaert, D. J. Conley, S. Van Damme, P. Meire, J. J. Middelburg, M. Vos, and E. Struyf. (2009). A macro-tidal freshwater ecosystem recovering from hypereutrophication: The Schelde case study. Biogeosciences 6:2935–2948. [doi:10.5194/bg-6-2935-2009].

Davidson, K., and W. S. C. Gurney. (1999). An investigation of non-steady-state algal growth. II. Mathematical modelling of co-nutrient-limited algal growth. J. Plankt. Res. 21:839–858. [doi:10.1093/plankt/21.5.839].

Flynn, K. J. (2003a). Do we need complex mechanistic photoacclimation models for phytoplankton? Limnol. Oceanogr. 48:2243–2249. [doi:10.4319/lo.2003.48.6.2243].

Flynn, K. J. (2003b). Modelling multi-nutrient interactions in phytoplankton; balancing simplicity and realism. Prog. Oceanogr. 56:249–279. [doi:10.1016/S0079-6611(03)00006-5].

Flynn, K. J., and V. Martin-Jezequel. (2000). Modelling Si-N-limited growth of diatoms. J. Plankt. Res. 22:447–472. [doi:10.1093/plankt/22.3.447].

Gazeau, F., J. P. Gattuso, J. J. Middelburg, N. Brion, L. S. Schiettecatte, M. Frankignoulle, and A. V. Borges. (2005). Planktonic and whole system metabolism in a nutrient-rich estuary (the Scheldt estuary). Estuaries 28:868–883. [doi:10.1007/BF02696016].

Geider, R. J., H. L., MacIntyre, and T. M. Kana. (1997). Dynamic model of phytoplankton growth and acclimation: Responses of the balanced growth rate and the chlorophyll a:carbon ratio to light, nutrient-limitation and temperature. Mar. Ecol. Prog. Ser. 148:187–200. [doi:10.3354/meps148187].

Goebel, N. L., and J. N. Kremer. (2007). Temporal and spatial variability of photosynthetic parameters and community respiration in long island sound. Mar. Ecol. Prog. Ser. 329:23–42. [doi:10.3354/meps329023].

Goosen, N. K., J. Kromkamp, J. Peene, P. van Rijswijk, and P. van Breugel. (1999). Bacterial and phytoplankton production in the maximum turbidity zone of three European estuaries: The Elbe, Westerschelde and Gironde. J. Mar. Syst. 22:151–171. [doi:10.1016/S0924-7963(99)00038-X].

Keller, A. A. (1988). An empirical-model of primary productivity (C-14) using mesocosm data along a nutrient gradient. J. Plankt. Res. 10:813–834. [doi:10.1093/plankt/10.4.813].

Kromkamp, J., and J. Peene. (1995). On the possibility of net primary production in the turbid Schelde estuary (SW Netherlands). Mar. Ecol. Prog. Ser. 121:249–259. [doi:10.3354/meps121249].

Lewitus, A., D. White, R. Tymowski, M. Geesey, S. Hymel, and P. Noble. (2005). Adapting the CHEMTAX method for assessing phytoplankton taxonomic composition in Southeastern U.S. estuaries. Estuaries 28:160–172. [doi:10.1007/BF02732761].

Lionard, M., K. Muylaert, M. Tackx, and W. Vyverman. (2008). Evaluation of the performance of HPLC-CHEMTAX analysis for determining phytoplankton biomass and composition in a turbid estuary (Schelde, Belgium). Estuar. Coast. Shelf Sci. 76:809–817. [doi:10.1016/j.ecss.2007.08.003].

Lippemeier, S., P. Hartig, and F. Colijn. (1999). Direct impact of silicate on the photosynthetic performance of the diatom *Thalassiosira weissflogii* assessed by on- and off-line PAM fluorescence measurements. J. Plankt. Res. 21:269–283. [doi:10.1093/plankt/21.2.269].

MacIntyre, H. L., and J. J. Cullen. (1996). Primary production by suspended and benthic microalgae in a turbid estuary: Time-scales of variability in San Antonio bay, Texas. Mar. Ecol. Prog. Ser. 145:245–268. [doi:10.3354/meps145245].

Mackey, M., D. Mackey, H. Higgins, and S. Wright. (1996). CHEMTAX—a program for estimating class abundance for chemical markers: Application to HPLC measurements of phytoplankton. Mar. Ecol. Prog. Ser. 144:265–283. [doi:10.3354/meps144265].

Martin-Jezequel, V., M. Hildebrand, and M. A. Brzezinski. (2000). Silicon metabolism in diatoms: Implications for growth. J. Phycol. 36:821–840. [doi:10.1046/j.1529-8817.2000.00019.x].

Meire, P., T. Ysebaert, S. Van Damme, E. Van den Bergh, T. Maris, and E. Struyf. (2005). The Scheldt estuary: A description of a changing ecosystem. Hydrobiologia 540:1–11. [doi:10.1007/s10750-005-0896-8].

Mizon, G. E. (1977). Inferential procedures in nonlinear models: Application in a UK industrial cross-section study of factor substitution and returns to scale. Econometrica 45:1221–1242. [doi:10.2307/1914069].

Morris, E., and J. Kromkamp. (2003). Influence of temperature on the relationship between oxygen- and fluorescence-based estimates of photosynthetic parameters in a marine benthic diatom (*Cylindrotheca closterium*). Eur. J. Phycol. 38:133–142. [doi:10.1080/0967026031000085832].

Muylaert, K., K. Sabbe, and W. Vyverman. (2000). Spatial and temporal dynamics of phytoplankton communities in a freshwater tidal estuary (Schelde, Belgium). Estuar. Coast. Shelf Sci. 50:673–689. [doi:10.1006/ecss.2000.0590].

Press, W. H., S. A. Teukolsky, W. T. Vetterling, and B. P. Flannery. (2003). Numerical recipes in Fortran 77: The art of scientific computing. Cambridge University Press.

R Development Core Team (2006). R: A language and environment for statistical computing. R Foundation for Statistical Computing, Vienna, Austria. ISBN 3-900051-07-0.

Schlüter, L., F. Møhlenberg, H. Havskum, and S. Larsen. (2000). The use of phytoplankton pigments for identifying and quantifying phytoplankton groups in coastal areas: Testing the influence of light and nutrients on pigment/chlorophyll a ratios. Mar. Ecol. Prog. Ser. 192:49–63. [doi:10.3354/meps192049].

Seber, G., and C. Wild. (1989). Nonlinear regression. Wiley series in probability and mathematical statistics. Applied probability and statistics. John Wiley and Sons.

Sobrino, C., and P. J. Neale. (2007). Short-term and long-term effects of temperature on photosynthesis in the diatom *Thalassiosira pseudonana* under UVR exposures. J. Phycol. 43:426–436. [doi:10.1111/j.1529-8817.2007.00344.x].

Steemann Nielsen, E. (1951). Measurement of the production of organic matter in the sea by means of carbon-14. Nature 167:684–685. [doi:10.1038/167684b0 PMid:14826912].

Strickland, J., and T. Parsons. (1972). A practical handbook of seawater analyses. Ottawa: Fisheries Research Board of Canada, 2nd edition.

Unesco (1985). The International System of Units (SI) in Oceanography. Unesco Technical Papers in Marine Science 45, Unesco, Paris.

Van Damme, S., E. Struyf, T. Maris, T. Ysebaert, F. Dehairs, M. Tackx, C. Heip, and P. Meire. (2005). Spatial and temporal patterns of water quality along the estuarine salinity gradient of the Scheldt estuary (Belgium and The Netherlands): Results of an integrated monitoring approach. Hydrobiologia 540:29–45. [doi:10.1007/s10750-004-7102-2].

Webb, W., M. Newton, and D. Starr. (1974). Carbon-dioxide exchange of Alnus-Rubra: Mathematical-model. Oecologia 17:281–291. [doi:10.1007/BF00345747].

Wright, S., and S. Jeffrey. (1997). High resolution system for chlorophylls and carotenoids of marine phytoplankton. In S. Jeffrey, R. Mantoura, and S. Wright (Eds.), Phytoplankton pigments in oceanography: A guide to advanced methods (pp. 327–341). Paris: SCOR-UNESCO.

Yentsch, C., and D. Menzel. (1963). A method for the determination of phytoplankton chlorophyll and phaeophytin by fluorescence. Deep-Sea Res. 221–231.

Submitted 12 January 2010
Revised 18 May 2010
Accepted 1 July 2010